Two-dimensional near-field and far-field imaging of a Ne-like Ar capillary discharge table-top soft-x-ray laser

C. H. Moreno,* M. C. Marconi,* V. N. Shlyaptsev,† B. R. Benware, C. D. Macchietto, J. L. A. Chilla, and J. J. Rocca
Electrical Engineering Department, Colorado State University, Fort Collins, Colorado 80523

A. L. Osterheld
Lawrence Livermore National Laboratory, Livermore, California 94551

We have performed systematic measurements and numerical modeling of the divergence and exit beam size of a 46.9 nm Ne-like Ar capillary discharge pumped soft-x-ray amplifier. Two-dimensional near-field and far-field measurements were obtained over a wide range of discharge parameters. The spot size and divergence of the laser beam were observed to increase significantly with decreasing discharge pressure. Simultaneously, the beam intensity distribution changed from a single peak pattern to an annular profile. These effects are shown to be the result of increased refraction of the soft-x-ray beam, caused by larger density gradients in the plasma columns of the lower pressure discharges. The spatial images are nearly cylindrically symmetric, and have less structure than those reported in the literature for laser-driven soft-x-ray lasers. Beam profiles synthesized by model calculations are found to be in good agreement with the recorded images. The obtained images in combination with the model computations clarify the origin of the different beam patterns that are observed in capillary discharge soft-x-ray laser experiments. [S1050-2947(98)09208-7]

PACS number(s): 42.55.Vc; 42.60.Jf

I. INTRODUCTION

The observation of large soft-x-ray amplification in the plasma of a capillary discharge [1] and the subsequent demonstration of a saturated discharge pumped table-top soft-x-ray laser in Ne-like Ar at 46.9 nm [2] have established a new approach for the development of compact and practical soft-x-ray lasers. In these lasers the gain medium is a hot and dense plasma column with aspect ratios approaching 1000:1, generated in a capillary channel by a fast discharge current pulse. The fast current pulse rapidly compresses the plasma to form a needle-shaped column in which lasing is obtained by collisional electron excitation of Ne-like ions [1–3]. Knowledge of the near-field and far-field spatial distribution of the output of these lasers is of both practical and basic interest. Significant insight in the physics of this new kind of soft-x-ray amplifier can be gained from such images. Recently, two-dimensional near-field imaging studies of the laser-pumped soft-x-ray amplifiers have been reported [4–7]. For example, near-field imaging studies of a laser-pumped Ne-like Ge soft-x-ray laser experimentally confirmed that lasing in the $J = 0 - 1$ line takes place closer to the target and in a higher density region as compared with the $J = 2 - 1$ line [4]. The images recorded in those studies have also shown that the soft-x-ray laser beams generated in that kind of laser-created plasmas have a great deal of structure [4,5].

Herein we report the results of a near-field imaging study

of a capillary discharge-pumped soft-x-ray laser, together with far-field two-dimensional images obtained for the same discharge conditions. Measurements performed decreasing the discharge pressure showed an important increase in laser beam refraction caused by larger density gradients in the plasma column. As the discharge pressure was lowered from 750 to 500 mTorr the beam diameter and divergence increased, and the beam profile was observed to change from a single peak distribution with the maximum on axis to an annular-shape profile. These observations are in good agreement with ray tracing model calculations that used the electron density and gain profiles computed with a hydrodynamic-atomic physics model of the plasma. The computations show that the plasmas of the lower pressure discharges have significantly larger density gradients, larger temperatures, and reduced radial opacity.

II. EXPERIMENTAL SETUP

The measurements were conducted in a Ne-like Ar capillary discharge laser emitting a single strong laser line at 46.9 nm [8]. In this device, a fast current pulse with a peak amplitude of about 37 kA having a first half period of 72 ns generates and compresses an elongated Ar plasma column in which the necessary conditions for lasing are achieved approximately 39 ns after the onset of the current. In the experiments we report herein, the discharges took place in a polyacetal capillary 16.4 cm long, 4 mm in diameter filled with pure Ar gas at different selected pressures ranging from 500 to 750 mTorr.

The imaging setup employed to record the near-field patterns is schematically illustrated in Fig. 1. The output aperture of the capillary discharge laser was imaged into a two-dimensional soft-x-ray sensitive detector using a 150 cm radius of curvature iridium-coated mirror. The curved mirror
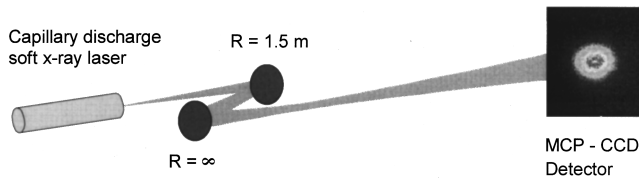

FIG. 1. Schematic representation of the setup used to obtain two-dimensional near-field images of the output of the capillary discharge Ne-like Ar laser.

was positioned at 82.1 cm from the exit of the capillary. A flat iridium-coated mirror was used between the curved mirror and the detector to relay the image. The reflectivity of the iridium mirrors used in this experiment was measured to be about 10% at 46.9 nm. The detector consisted of a microchannel plate followed by a phosphor screen, an image intensifer and a charged-coupled-device (CCD) array of 1024 ×1024 pixels 24.8 μm wide. A thin Al film was evaporated on the phosphor screen to avoid the detection of visible plasma radiation. The microchannel plate was gated for about 5 ns to differentiate the laser radiation, which is emitted in a ≈0.7-ns-wide pulse, from the much less intense but long lasting (>100 ns) soft-x-ray radiation spontaneously emitted by the discharge. The voltage of the gate pulse was maintained low (150 V) to avoid saturation of the detector. The linearity of the detection system was experimentally verified. The curved mirror imaged the output of the laser on the detector plane with a magnification of ≈10×. However, the optics used to image the phosphorous screen on the CCD array demagnified the image, resulting in a total effective magnification of 8× for the system. The spatial resolution of the entire imaging system was determined to be approximately 16 μm in the object plane by imaging an array of 25 μm diameter holes placed at the exit plane of the capillary channel. The same measurement allowed for a direct experimental calibration of the magnification of the imaging system. To record the far-field images the iridium-coated mirrors were removed and the detector was placed directly in front of the laser, at a distance of 148 cm from the exit of the capillary.

III. EXPERIMENTAL RESULTS

We recorded two-dimensional near-field images of the output of the laser as a function of Ar pressure. Figure 2(a) shows the result of a series of measurements for discharge pressures between 500 and 750 mTorr obtained with a discharge current of 37 kA. This current was selected because it is nearly the optimum for maximum laser output energy extraction. At the higher pressures (>650 mTorr) the near-field laser beam distribution is observed to consist of a single circular peak with maximum intensity at the center and monotonically decreasing intensity towards the periphery. As the pressure decreases, the beam size at the exit of the amplifier gets increasingly larger, and finally develops into a ring structure. At a pressure of ≅500 mTorr the intensity at the periphery dominates the beam profile. The FWHM beam diameter at the exit of the amplifier was measured to increase from about 150 μm at 750 mTorr to about 300 μm at 500 mTorr. The far-field measurements and model computations discussed below show that these effects are caused by larger

refraction of the beam in the lower pressure discharges. We have observed that the pressure at which the beam intensity distribution makes a transition from a single peak profile to a ring structure can vary from one capillary to another by as much as 100 mTorr. For a given discharge pressure the shape of the beam pattern was observed to be relatively insensitive to the current within the range investigated (32.5 to 41 kA). It should be noticed that the near-field patterns, in particular those corresponding to the higher pressure results, are more homogeneous and have significantly less structure than those that have been reported for laser-pumped amplifiers [4,5]. Near-field images were also recorded for shorter capillaries, for which refraction is less significant in determining the intensity profile. We observed that while for low-pressure discharges in capillaries 16.4 cm in length the near-field pattern had an annular shape, for 11.5-cm-long columns the profile typically had a dominant central peak, as shown in Fig. 3. For the short capillaries a significant ring structure was only observed in shots at currents greater than 41 kA.

Figure 2(b) shows the far-field beam patterns corresponding to each of the discharge conditions of the near-field patterns of Fig. 2(a). As in the case of the near-field images, a transformation is observed in the spatial intensity distribution from a beam profile with a single peak at the center to a ring profile, as the pressure is decreased. A ring structure is again observed for the discharges at pressures <550 mTorr. This is accompanied by an increase in the beam divergence, from about 2 mrad for discharges at 750 mTorr to about 5 mrad for discharges at 500 mTorr. These results show that refraction increases as the pressure is decreased.

To obtain a more complete picture of the output characteristics of this laser these data need to be considered in combination with the variation of the laser output energy. Figure 4 shows the dependence of the laser output energy with the pressure, obtained by integrating the intensity for each of the far-field images. The maximum laser output energy is observed for pressures near 580 mTorr. At pressures either below 450 mTorr or above 750 mTorr, the laser output energy at this discharge current rapidly vanishes. It is observed that for pressures down to about 600 mTorr the laser output energy increases with decreasing pressure in spite of the increase in refraction. This indicates that within this pressure range there is an increase in the gain with decreasing pressure, which more than compensates for the larger refraction losses.

IV. COMPARISON WITH MODEL CALCULATIONS AND CONCLUSIONS

The measurements were analyzed in comparison with the results of model computations for this Ne-like Ar capillary discharge pumped amplifier. The simulations were conducted with the hydrodynamic-atomic physics code RADEX [2,9,10], using self-consistent nonlocal thermodynamical equilibrium atomic physics in the transient approximation, with radial radiation transport and postprocessor axial ray tracing. Near-field and far-field laser images for the discharge conditions of the experiments described in the preceding section were calculated with a ray tracing code that computes the trajectory and the variation of the intensity
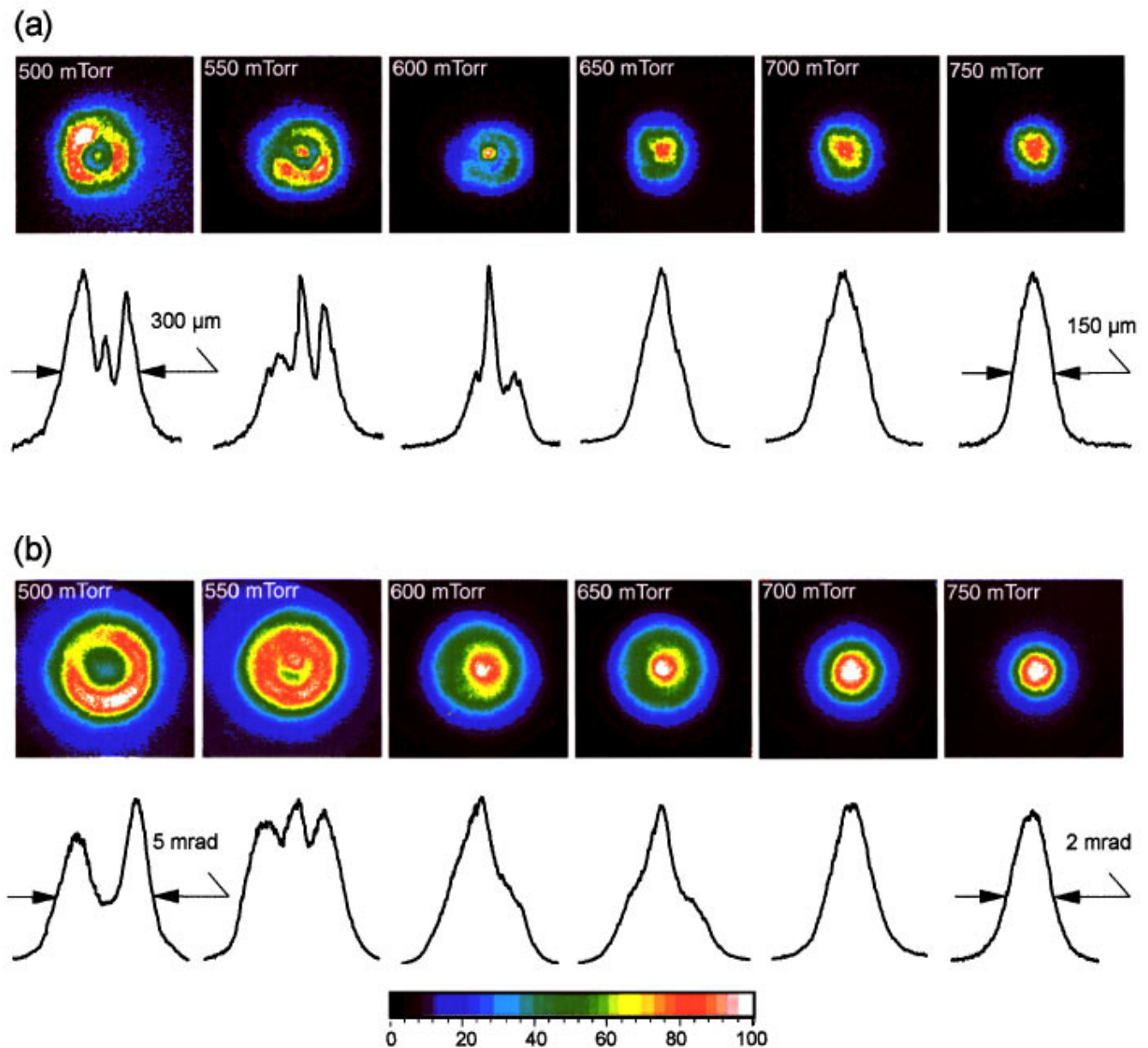
(a)

(b)

FIG. 2. (Color) Near-field (a) and far-field (b) images of the output of the 46.9 nm capillary discharge pumped Ne-like Ar laser as a function of pressure. The measurements correspond to a 16.4-cm-long, 4-mm-diameter capillary excited by a 37 kA current pulse. In each case a corresponding cut of the profile along the vertical axis is shown with normalized amplitude. The pseudocolor scale only indicates the relative intensities within each image. For the variation of the laser energy with pressure, see Fig. 4.

associated with rays that propagate along the capillary plasma column. The ray tracing calculations made use of the gain and plasma density spatiotemporal distributions supplied by the hydrodynamic and atomic physics parts of the code.

Figures 5(a) and 5(b) show cross sections of the computed near-field and far-field profiles respectively as a function of the discharge pressure. A comparison of these cross sections with those of Fig. 2 shows in general a good agreement between the results of the model and the experiment. The model clearly reproduces the experimentally observed evolution of the laser output from a low divergence beam with a single peak profile at a pressure of 750 mTorr into a larger divergence beam with a ring structure at lower pressures. The near-field size and far-field divergence of the computed
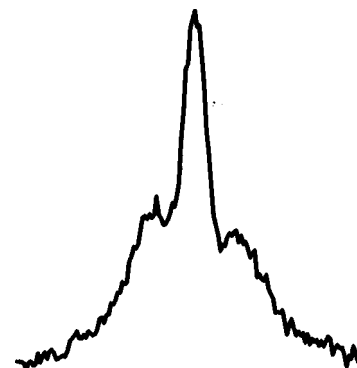

FIG. 3. Near-field image of the laser output corresponding to a 11.5-cm-length capillary at a discharge pressure of 500 mTorr. The current is 37 kA.
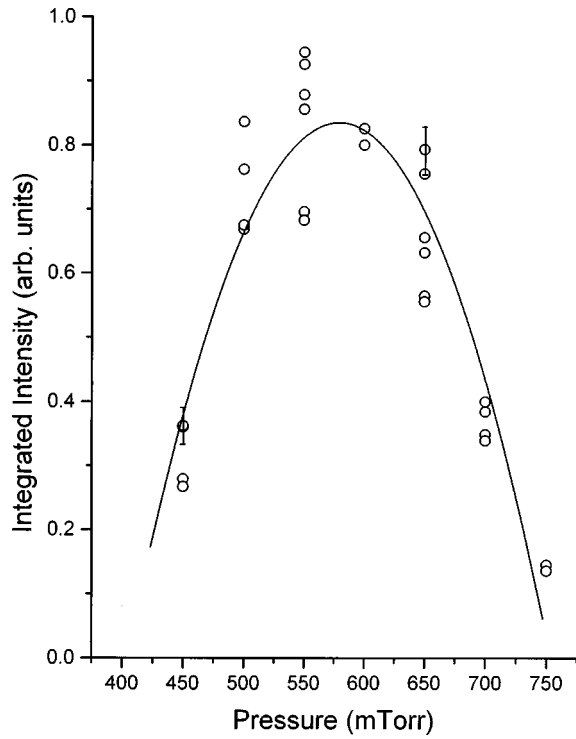
FIG. 4. Relative variation of the laser output energy as a function of the initial discharge pressure. The data was obtained integrating the far-field images of Fig. 2 and others in the same series of measurements. The solid line is a quadratic fit to the data. The error bars correspond to the uncertainty in determining the relative laser output energy from the far-field images of Fig. 2.
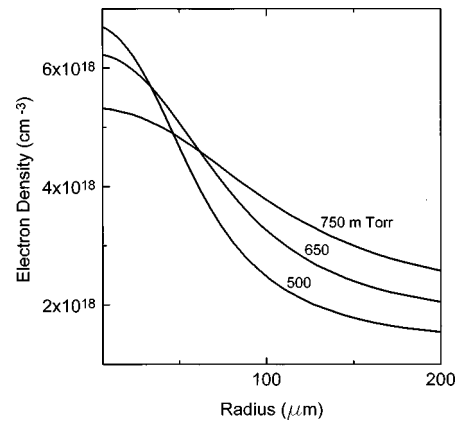

FIG. 6. Computed electron density profiles at three different pressures illustrating the larger density gradients associated with the lower pressure discharges. The computations correspond to a discharge current or 37 kA and to approximately the time of maximum soft x-ray laser pulse intensity. (For these discharge conditions the computed lasing times lie between 36 and 39 ns.)

beam profiles are also similar to those measured. The narrow central peak observed in the near-field images of the low-pressure discharges, which contains only about 2% of the laser output energy, is not present in the calculated profiles. This feature, which corresponds to highly collimated rays that are gain-guided through a very small central region of the plasma, is difficult to reproduce due to present numerical

limitations in the minimum size of computational grid.

The calculations and the observed near-field profiles for the short capillaries show that for these discharge conditions the amplification takes place in the vicinity of the axis of the capillary, where the gain coefficient is close to its maximum. This eliminates the possibility that annular near-field images might reflect similar annular gain distribution or annular density and temperature inhomogeneities. The calculations also show that beam refraction dramatically increases with decreasing pressure as a consequence of larger plasma density gradients in the capillary plasma column. Figure 6 shows the computed plasma density distribution near the axis at the time of maximum laser emission for three different pressures between 500 and 750 mTorr. It can be seen that at low pressures larger plasma density gradients are generated as the result of higher compressions that produce reduced final plasma column diameters and higher electron densities.
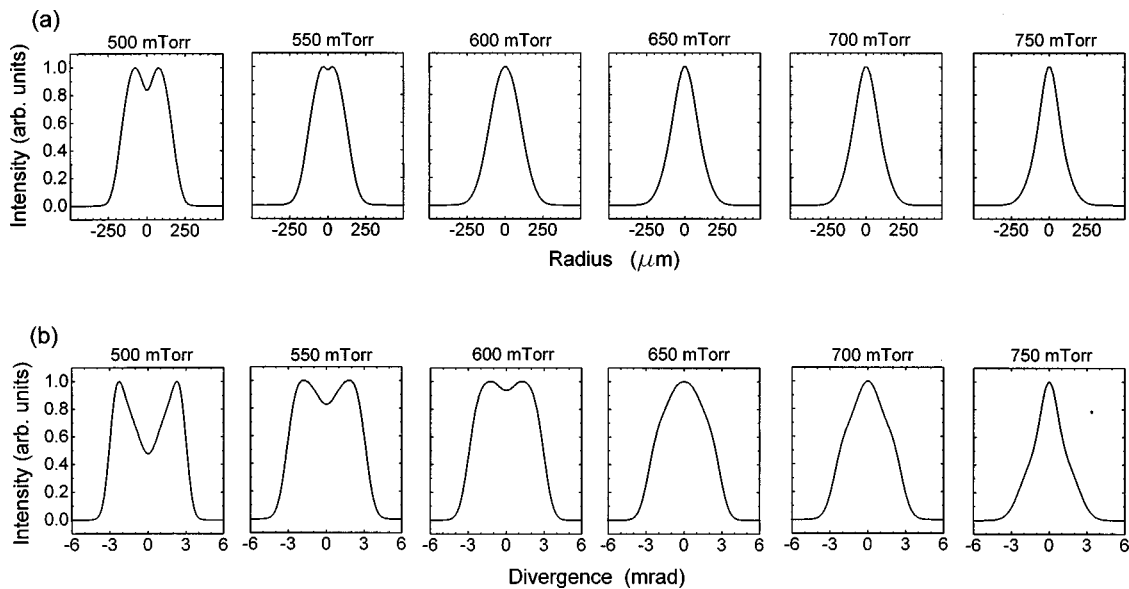

FIG. 5. Computed near-field (a) and far-field (b) beam profiles as a function of pressure for the discharge conditions of Fig. 2. The intensities are normalized to facilitate comparison.
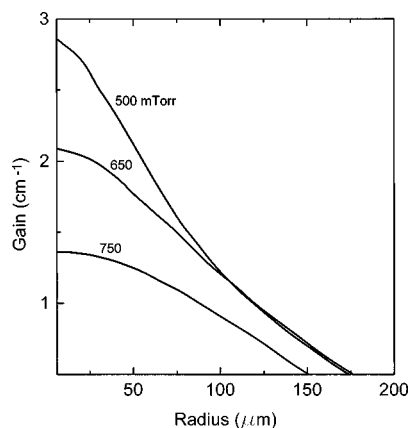
FIG. 7. Computed variation of the radial distribution of the small signal gain coefficient at three different values of the Ar pressure for a current of 37 kA. Notice that the *effective* gain coefficient is significantly smaller than the small signal gain values shown due to refraction losses. This reduction is larger at the lower pressures, where refraction is more important and the gain duration is shorter.

The calculations show that while refraction losses become larger as the pressure is decreased, the gain coefficient also increases. The computed variation of the radial distribution of the small signal gain coefficient at the time of maximum laser intensity for each of the three pressures is given in Fig. 7. The gain is larger at lower pressures due to an increase in electron temperature, a higher optimum plasma density for amplification and reduced opacity of the $3s$-$2p$ resonant lines [10,11]. Figure 8 shows the computed electron temperature profiles at the time of maximum laser intensity at different pressures. The electron temperature, which is calculated to be even significantly more homogeneous in space than the electron density, is computed to increase from about 65 eV at 750 mTorr to about 90 eV at 500 mTorr. This rise of the electron temperature contributes to increase the gain by increasing the pumping rate to the upper laser level, and by shifting the optimum electron density for amplification to higher values due to decreased collisional mixing between the laser levels. The reduced $3s$-$2p$ opacity is the result of the smaller plasma column diameter, and of a higher plasma velocity that causes increased Doppler detuning in the radial direction [10]. As the pressure is dropped from 750 to about 580 mTorr, the increase in the gain coefficient more than compensates for the increase in refraction losses, resulting in the increased laser output intensity shown in Fig. 4. However, as the pressure is further decreased, the increase in refraction losses becomes more important than the increase in the gain coefficient, and the overall result is the degradation of the laser output. Also contributing to a decreased laser output at the low end of the pressure range is the shorter duration of the gain, which gradually decreases from about 2.5 ns at 600 mTorr to a value that at 300–400 mTorr approaches the propagation time of the photons along the 16.4-cm-long amplifier, $Pt \cong 0.5$ ns. A further reduction of the pressure results in electron temperatures >90 eV and in near complete ionization of the Ne-like ions, finally quenching the gain.

This scenario, in which the described self-consistent variation of the plasma parameters explains the observed increase in the beam divergence at the lower pressures, is also
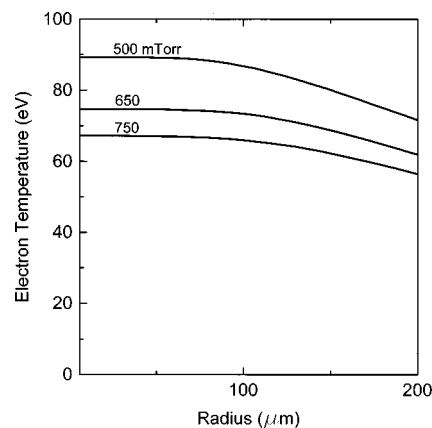

FIG. 8. Computed radial profiles of the electron temperature at the discharge conditions of Fig. 6.

valid at the high end of the pressure range where smaller density gradients result in a reduced beam divergence. At 750 mTorr the beam divergence starts to approach the value determined by the geometrical dimensions of the gain medium and diffraction. However, this is accompanied by a large decrease of the laser output energy as the result of a reduction in the gain coefficient. This reduction in the gain is in turn caused by a decrease in the electron temperature and optimum electron density, and by an increase in the radial opacity (the latter is again associated with increased plasma column diameter and a reduced influence of the motional Doppler shift).

In reference to the near-field images it should be noticed that the observed increase in spot size with decreasing pressure occurs in spite of the computed reduction in the size of the gain region. This indicates that refraction, which determines the far-field distribution, is also the dominant effect shaping the near-field intensity distribution. Confirmation of the importance of refraction is given by the fact that while for the 16.4-cm-long capillaries the low pressure near-field profiles are annular, those for the short capillaries (where refraction is a less significant factor) are typically dominated by a central peak.

In conclusion, we have obtained the first two-dimensional near-field images of the output of a discharge pumped soft-x-ray laser, for a 46.9 nm Ne-like argon amplifier. These images have the axial symmetry that is expected from a well-behaved capillary discharge. The near-field images corresponding to the higher pressure discharges present significantly less structure than those recently reported for laser-driven soft-x-ray lasers [4,5]. These measurements are a corroboration of the very high compression axial symmetry and plasma uniformity that is obtained in fast capillary discharges with lengths-to-diameter ratios approaching 1000:1. The images show that refraction is responsible for increasing the size and divergence of the beam from about 150 to 300 μm at the exit of the amplifier and from 2 to 5 mrad respectively as the discharge pressure is decreased from 750 to 500 mTorr, in good accordance with the calculations. The model shows that beam refraction and the gain coefficient both increase as the pressure is reduced. The former mostly due to reduced plasma size, and the latter as a consequence of larger temperatures, higher optimum densities, and reduced opacity at the time of lasing. Refraction was found to strongly influ

ence the intensity behavior of this capillary discharge laser and its near- and far-field profiles, as was already known to be the case in laser-driven soft-x-ray lasers with much higher electron densities.

In addition, it can be concluded that refraction can often overshadow the characteristics of the gain region in shaping the near-field patterns. Illustrations of this are our near-field measurements with decreasing pressure in the 16.4-cm-long Ne-like Ar capillary discharge amplifier, in which the size of the near-field pattern is observed to increase remarkably in spite of a decrease in the size of the gain region, and the recent measurements in laser-pumped soft-x-ray lasers [5].

[1] J. J. Rocca, V. N. Shlyaptsev, F. G. Tomasel, O. D. Cortazar, D. Hartshorn, and J. L. A. Chilla, Phys. Rev. Lett. **73**, 2192 (1994).

[2] J. J. Roca, D. P. Clark, J. L. A. Chilla, and V. N. Shlyaptsev, Phys. Rev. Lett. **77**, 1476 (1996).

[3] F. G. Tomasel, J. J. Rocca, V. N. Shlyaptsev, and C. D. Macchietto, Phys. Rev. A **55**, 1437 (1997).

[4] J. C. Moreno, J. Nilsen, Y. L. Li, P. X. Lu, and E. E. Fill, Opt. Lett. **21**, 866 (1996).

[5] J. Nilsen, J. C. Moreno, L. B. Da Silva, and T. W. Barbee, Jr., Phys. Rev. A **55**, 827 (1997).

[6] J. Nilsen, J. Zhang, A. G. MacPhee, J. Lin, T. W. Barbee, Jr., C. Danson, L. B. Da Silva, M. H. Key, C. L. S. Lewis, D. Neely, R. M. N. O'Rourke, G. J. Pert, R. Smith, G. J. Tallents,

J. S. Wark, and E. Wolfrum, Phys. Rev. A **56**, 3161 (1997).

[7] J. Zhang, J. Warwick, E. Wolfrum, M. Key, C. Danson, A. Demir, S. Healy, D. Kalantar, N. Kim, C. Lewis, J. Lin, A. MacPhee, D. Neely, J. Nilsen, G. Pert, R. Smith, G. Tallents, and J. Wark, Phys. Rev. A **54**, 4653 (1996).

[8] B. R. Benware, C. H. Moreno, D. J. Burd, and J. J. Rocca, Opt. Lett. **22**, 796 (1997).

[9] V. N. Shlyaptsev, A. V. Gerusov, A. V. Vinogradov, J. J. Rocca, O. D. Cortazar, F. T. Tomasel, and B. T. Szapiro, SPIE J. **2012**, 99 (1993).

[10] V. N. Shlyaptsev, J. J. Rocca, and A. L. Osterheld, SPIE J. **2520**, 365 (1995).

[11] A. V. Vinogradov and V. N. Shlyaptsev, Sov. J. Quantum Electron. **13**, 303 (1983).